Lithium Abundances in Giants as a Function of Stellar Mass: Evidence for He Flash as the Source of Li Enhancement in Low-mass Giants

Anohita Mallick[1,2] , Raghubar Singh[3] , and Bacham E. Reddy[1]

[1] Indian Institute of Astrophysics, 560034, 100ft Road, Koramangala, Bangalore, India; anohitamallick@gmail.com
[2] Pondicherry University, R.V. Nagara, Kala Pet, 605014, Puducherry, India
[3] Aryabhatta Research Institute of Observational Sciences (ARIES), Manora Peak, Nainital 263001, India

Abstract

In this work, we studied the distribution of lithium abundances in giants as a function of stellar mass. We used a sample of 1240 giants common among Kepler photometric and LAMOST medium-resolution ($R \approx 7500$) spectroscopic survey fields. The asteroseismic ΔP–$\Delta \nu$ diagram is used to define core He-burning red clump giants and red giant branch stars with an inert He core. Li abundances have been derived using spectral synthesis for all sample stars. Directly measured values of asteroseismic parameters ΔP (or $\Delta \Pi_1$) and $\Delta \nu$ are either taken from the literature or measured in this study. Of the 777 identified red clump giants, we found 668 low-mass ($\leqslant 2 M_\odot$) primary red clump giants and 109 high-mass ($> 2 M_\odot$) secondary red clump giants. Observed Li abundances in secondary red clump giants agree with the theoretical model predictions. The lack of Li-rich giants among secondary red clump giants and the presence of Li-rich, including super Li-rich, giants among primary red clump stars reinforces the idea that helium flash holds the key for Li enrichment among low-mass giants. The results will further constrain theoretical models searching for a physical mechanism for Li enhancement among low-mass red clump giants. Results also serve as observational evidence that only giants with mass less than $\approx 2 M_\odot$ develop a degenerate He core and undergo He flash.

Unified Astronomy Thesaurus concepts: Stellar abundances (1577); Red giant clump (1370); Helium burning (716); Asteroseismology (73)

Supporting material: machine-readable table

1. Introduction

It is well understood that stars on the red giant branch (RGB) undergo convective mixing or the first dredge-up, which alters photospheric abundances of several elements like helium, carbon, nitrogen, and lithium. Of those, Li is the most affected element. The surface Li abundance, $A(\text{Li})$, drops to ~95% of their main-sequence value (Iben 1967). The discovery of the first Li-rich giant (LRG; Wallerstein & Sneden 1982) four decades ago challenged the general understanding of Li evolution. Since then, numerous works (Brown et al. 1989; Kumar et al. 2011; Martell & Shetrone 2013; Casey et al. 2019; Deepak & Reddy 2019) established that a small fraction (~1%) of giants exhibit high levels of Li abundances compared to standard model predictions of $A(\text{Li}) = 1.5$–1.8 dex depending on mass. In many cases, the enhancement surpasses the primordial $A(\text{Li}) \simeq 2.7$ dex, and in a few cases, $A(\text{Li})$ is more than the present interstellar medium value of ~3.2 dex, which is tagged as super lithium-rich (SLR) stars. The existence of such stars transcends standard evolutionary theories, implying some ancillary mechanism behind the production and preservation of Li in LRGs. Various theories were proposed to explain the mechanism and site of Li production in giants, which include in situ production and an external origin (Boothroyd & Juliana Sackmann 1999; Charbonnel & Balachandran 2000; Charbonnel & Zahn 2007; Denissenkov et al. 2009; Carlberg et al. 2012).

While the Li origin debate was underway, a large observational study by Kumar et al. (2011) hypothesized that Li enhancement might be associated with red clump (RC) stars with a helium-burning core. Lithium synthesized in the interior by a process known as the Cameron–Fowler mechanism (Cameron & Fowler 1971) might have mixed up with the outer layers by noncanonical processes during the helium flash—a runaway nuclear burning at the RGB tip in low-mass stars ($\leqslant 2 M_\odot$). Now, hundreds of LRGs exist in the literature primarily due to large systematic studies (Casey et al. 2019; Deepak & Reddy 2019; Singh et al. 2019; Martell et al. 2021; Yan et al. 2021) based on large spectroscopic surveys such as LAMOST and GALAH and the space-based data sets of Gaia astrometry and time-resolved photometry from Kepler and TESS. Also, these studies concluded that most LRGs belong to the He-core-burning RC phase. The study by Kumar et al. (2020) demonstrated that Li enhancement is ubiquitous among core He-burning low-mass RC giants, and Li gets only depleted in giants ascending the RGB, implying He flash at the RGB tip is the most likely cause for Li enhancement among RC giants. Further, Singh et al. (2021), using Li abundances and asteroseismic parameters, showed that most of the SLR giants are very young RCs compared to Li-normal RC giants, implying Li enhancement in SLRs occurred very recently. A recent observational study by Sneden et al. (2022) showed that Li-rich giants are more likely to have a strong chromospheric He line at 10830 Å opening a new avenue to probe THE Li-rich origin. These observational results are yet to be supported by theoretical modeling. One of the physical mechanisms proposed for Li enhancement is extra mixing due to the excitation of internal gravity waves by turbulent convection
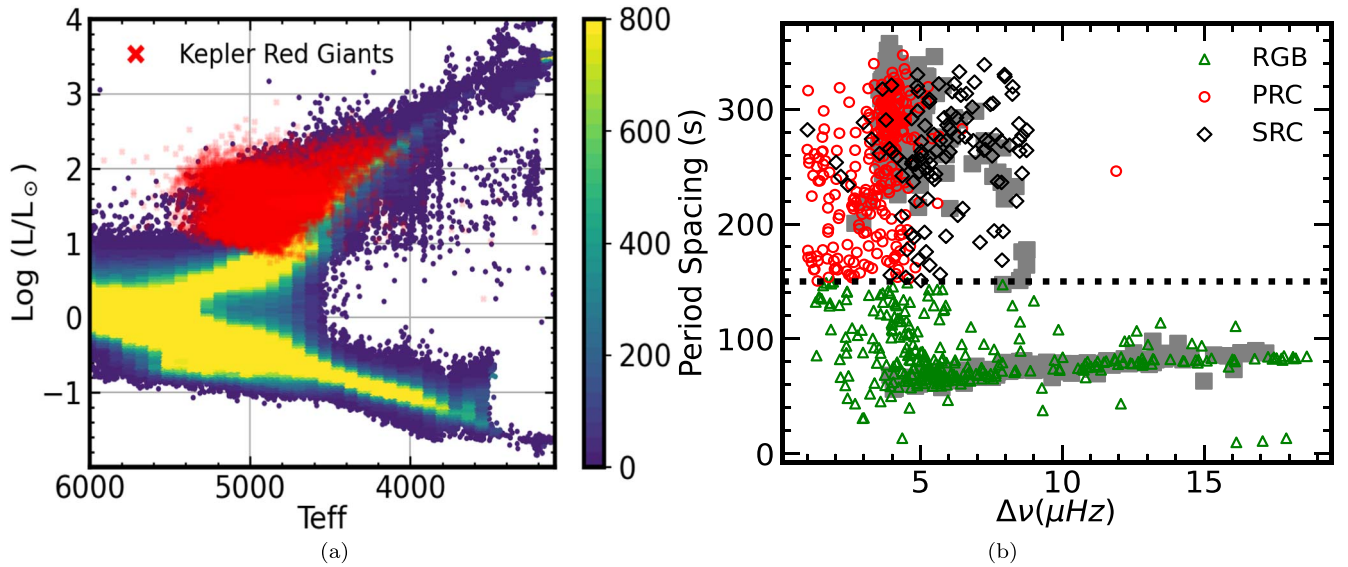
Figure 1. Shown are the sample giants of RC and RGB. In panel (a), 16,094 stars (red symbols) from Yu et al. (2018) are plotted with the entire Kepler sample as background. In panel (b), asteroseismically classified RGB and RC sample stars in this study are shown along with the sample giants from Vrard et al. (2016).

caused by the He flash and the associated large luminosity (Schwab 2020a).

There are still questions related to the high-Li origin in giants. Is the He flash a universal production mechanism for Li? Does Li enhancement occur only in low-mass giants, or are there massive ($>2\,M_\odot$) Li-rich giants as well? Until now, surveys focused mostly on low-mass RC giants at the cooler end of the horizontal branch (HB). It would be interesting to map LRGs over a range of masses to understand the origin of Li enhancement. This is because if He flash is the sole mechanism for high Li in giants, one would not expect LRGs among high-mass giants as He-flash is expected to occur only in low-mass ($\leqslant 2\,M_\odot$) giants. Recently, the two observational studies (Martell et al. 2021; Zhou et al. 2022) showed the presence of LRGs across mass and evolutionary phases, implying Li enhancement in giants could be from multiple sites. However, both studies suffer from ambiguity in determining giants' evolutionary phase due to a lack of direct measurement of asteroseismic parameters.

Here, we assembled one of the largest data sets of 1240 giants for which direct measurements of asteroseismic parameters and LAMOST medium-resolution spectra are available. The maximum initial mass of a star ($M_{\rm HeF}$) to experience a He flash ranges from 1.8 to $2.2\,M_\odot$ depending on its metallicity (Chiosi et al. 1992). In this study, we probed Li abundance patterns as a function of mass among RC giants. In particular, among the "secondary RC stars" using a cutoff mass $M_{\rm HeF} > 2\,M_\odot$.

2. Sample Selection

It is challenging to unambiguously identify giants' evolutionary phase, particularly the He-core-burning RC giants from those ascending the RGB, solely by their location on the $T_{\rm eff}-L$ diagram (HRD). It is because the luminosity bump and upper RGB overlap with the RC regions. It is essential to have an independent way of knowing stars' evolutionary phases, either as RC or RGB giants. The Kepler space mission data provide the high-quality and high-cadence time-resolved photometry required for asteroseismic analysis. RC and RGB giants show

characteristic oscillation properties enabling one to separate RC giants from those on RGB (Bedding et al. 2011).

We adopted a sample of 16,094 giants from the catalog by Yu et al. (2018), who compiled giants for which oscillations were detected. It contains only stars with log $g \geqslant 1.5$ or log $(L/L_\odot) \leqslant 2.24$ dex, i.e., only RC and RGB giants. The catalog excluded stars with the frequency of the maximum oscillation power, $\nu_{\rm max} < 5\,\mu$Hz and $\nu_{\rm max} \geqslant 275\,\mu$Hz. The lower value culls out super giants, and the higher limit excludes dwarfs and subgiants. This sample is shown in the HRD (Figure 1(a)) with the entire Kepler data as background. The sample's luminosity values are estimated using stellar parallax, and values of apparent magnitude are taken from the Gaia DR3 catalog. One could notice giants in the well-defined RC region in the HRD. Yu et al. (2018) provided asteroseismic parameters ($\nu_{\rm max}$, $\Delta\nu_{\rm max}$) and stellar parameters (mass, radius, log g, [Fe/H]) for the entire sample based on a homogeneous asteroseismic analysis.

Our main focus in this study is to understand the distribution of Li among giants as a function of mass. For this, we cross-matched the Yu et al. (2018) sample with the LAMOST medium-resolution spectroscopic survey DR7 catalog (Luo et al. 2022). We found 1240 giants common between the two catalogs. All the giants have reasonably good spectra with signal-to-noise ratio (S/N) $\geqslant 30$. Most of the spectra (88%) have S/N > 50. For the classification of giants as RC or RGB, we turned to the literature because the Yu et al. (2018) catalog did not provide mixed-mode period-spacing (ΔP) values. Their classification is based on $\nu_{\rm max}$ and $\Delta\nu$ (see their Figure 7). We have not adopted this method as there may be a possibility of contamination of RCs with RGB or vice versa, particularly at lower $\Delta\nu$ ($<10\,\mu$Hz). To minimize contamination, we adopted directly measured values of $\Delta\Pi_1$ from the literature (Vrard et al. 2016; Singh et al. 2019). We found $\Delta\Pi_1$ values for 584 giants. For the remaining 656 giants, the ΔP values are calculated in this study using Kepler light curves (see Appendix A). The 1240 giants will be our working sample for this study, and the sample is shown in the asteroseismic diagram of ΔP versus $\Delta\nu$ along with the sample of RC and RGBs classified by Vrard et al. (2016) as background. Going

by the convention, we classified giants with ΔP(or $\Delta\Pi_1$) $\geqslant 150$ s as RC giants and giants with ΔP(or $\Delta\Pi_1$) < 150 s as RGB giants. The ΔP demarcation divides the sample into 777 RC giants and 463 RGB giants. Small contamination cannot be ruled out as there is a small overlap of RC and RGB space in the ΔP–$\Delta\nu$ diagram, particularly at $\Delta\nu \approx 5\,\mu$Hz. However, as the sample in Figure 1(b) suggests, the RC sample with $\Delta P \geqslant 150$ s may be least contaminated with the RGB sample as the RC sample cutoff at ΔP is $\approx 3\sigma$ away from the mean trend of the RGB in the plot.

3. Analysis

Our primary goal in this study is to understand Li abundances among RC giants with a range of stellar masses.

3.1. Stellar-mass Estimation

The traditional method of using evolutionary tracks for mass determination may not yield desired results as tracks degenerate at RC and RGB regions. The scaling relations based on asteroseismic parameters are found to be useful for individual stellar masses. The study by Yu et al. (2018) provides estimated masses using the revised scaled relations (Sharma et al. 2016). Here, we provide a brief account:

$$\frac{M}{M_\odot} = \left(\frac{\nu_{\max}}{f_{\nu_{\max}}\,\nu_{\max,\odot}}\right)^3 \left(\frac{\Delta\nu}{f_{\Delta\nu}\,\Delta\nu_\odot}\right)^{-4} \left(\frac{T_{\rm eff}}{T_{\rm eff,\odot}}\right)^{1.5}, \quad (1)$$

where $f_{\nu_{\max}}$ and $f_{\Delta\nu}$ are correction factors for the $\nu_{\max}$ and $\Delta\nu$ scaling relations. For our work, we used $f_{\nu_{\max}} = 1.0$, and $f_{\Delta\nu}$ was calculated from the ASFGRID code by Sharma et al. (2016). The solar reference values are $\nu_{\max,\odot} = 135.1\,\mu$Hz, $\Delta\nu_\odot = 3090\,\mu$Hz, and $T_{\rm eff,\odot} = 5777$ K, respectively. The asteroseismic parameters $\nu_{\max}$, $\Delta\nu$, and $T_{\rm eff}$ are taken from Yu et al. (2018). We have divided the RC sample into two broad groups based on their mass: the low-mass ($\leqslant 2\,M_\odot$) RC giants or the primary RC giants (pRCs) and high-mass ($>2\,M_\odot$) RC giants or secondary RC giants (sRCs). Similarly, we divided the RGB sample into two mass groups: massive RGB and low-mass RGB giants. We used the demarcation at $2\,M_\odot$ as only giants below this mass limit are expected to develop degenerate cores on the RGB. There are 668 pRCs, 109 sRCs, 10 massive RGBs, and 453 low-mass RGBs. A significantly smaller number of high-mass giants in the sample may be due to evolutionary timescales as high-mass giants evolve much faster compared to lower-mass giants.

3.2. Li Abundances

We have extracted spectra of the entire sample of 1240 giants from the LAMOST DR7 survey. Most of the spectra are of good quality with S/N $\geqslant 50$. Few spectra have lower S/N but are sufficient for deriving abundances using synthesis. All spectra are continuum fitted and radial velocity (RV) corrected using the estimated radial velocity data from the LAMOST catalog using tasks in IRAF. We used the spectral synthesis method to account for the blending of lines with the main Li resonance line at 6707 Å. The stellar parameters $T_{\rm eff}$, log g, and [Fe/H] are adapted from the Yu et al. (2018) catalog. The values of microturbulent velocity (ξ) have been derived using the empirical relation for giants with [Fe/H] > -1.0 dex

(Holtzman et al. 2018):

$$\xi = 10^{0.226 - 0.0228\log g + 0.0297(\log g)^2 - 0.0113(\log g)^3},$$

and for giants with [Fe/H] $\leqslant -1.0$ dex (García Pérez et al. 2016):

$$\xi = 2.478 - 0.325\log g.$$

The required line list and associated atomic and molecular data were collated by the linemake code (Placco et al. 2021) around the Li I line at 6707.8 Å. Local thermodynamic equilibrium (LTE) model atmospheres were generated from the ATLAS9 code (Castelli & Kurucz 2003) for the adopted atmospheric parameters. A series of synthetic spectra was generated using the updated 2019 version of the radiative transfer code MOOG (Sneden 1973) for each program star by changing Li abundances. The predicted spectra were then matched with the observed spectra. Li abundance of the best-matched (least χ-squares) computed spectrum was taken as the star's Li abundance. The S/Ns of spectra were adapted from the mean R-band S/N supplied by the LAMOST stellar parameter pipeline (LASP; Xiang et al. 2015). To estimate the effect of the S/N on abundance measurements, we calculated errors in equivalent widths using Cayrel's formula (Cayrel 1988). The weakest lines in our spectra (S/N range from 30 to 838) that can be detected have EWs 0.62–17.5 mÅ. We used a 3σ limit on the EWs for reliable abundance measurements. This renders a detection limit of EW = 1.88–52.4 mÅ, equivalent to A(Li) limits of 0.2–0.9 dex, depending on $T_{\rm eff}$ and log g. All sample giants have A(Li) well above the detection threshold. A sample synthetic spectrum comparison with the observed spectra is given in Figure 2. The third spectrum in the panel has one of the lowest S/N ≈ 30. Since these giants are cool, the Li resonance line is normally very strong even for giants with moderate Li abundances. Uncertainties in the Li abundance are calculated using a quadratic sum of uncertainties attributable to the spectral quality and stellar parameters and are estimated as follows:

$$\Delta A({\rm Li})$$
$$= \sqrt{\Delta A(Li)_{\rm S/N}^2 + \Delta A(Li)_{T_{\rm eff}}^2 + \Delta A({\rm Li})_{\rm [Fe/H]}^2 + \Delta A(Li)_\xi^2},$$

where

$$\Delta A({\rm Li})_{\rm S/N} = a_0 + a_1 \times {\rm S/N}$$

is due to uncertainties in S/N,

$$\Delta A({\rm Li})_{T_{\rm eff}} = b_0 + b_1 \times T_{\rm eff} + b_2 \times T_{\rm eff}^2 + b_3 \times T_{\rm eff}^3$$

is due to uncertainties in $T_{\rm eff}$,

$$\Delta A({\rm Li})_{\rm [Fe/H]} = c_0 + c_1 \times {\rm [Fe/H]} + c_2 \times {\rm [Fe/H]}^2 + c_3 \times {\rm [Fe/H]}^3$$

is due to uncertainties in [Fe/H], and

$$\Delta A({\rm Li})_\xi = d_0 + d_1 \times \xi$$

is due to uncertainties in ξ. Here a_i, b_i, c_i, and d_i are polynomial coefficients adapted from Gao et al. (2021). We also provided NLTE corrections for the Li abundances, utilizing $\Delta_{\rm NLTE}$ values from Lind et al. (2009). Parameters and abundances of all sample giants have been provided in Table 1. There are 18 giants in our sample for which Li abundances were derived from high-resolution spectra in the literature (Yan et al. 2021).
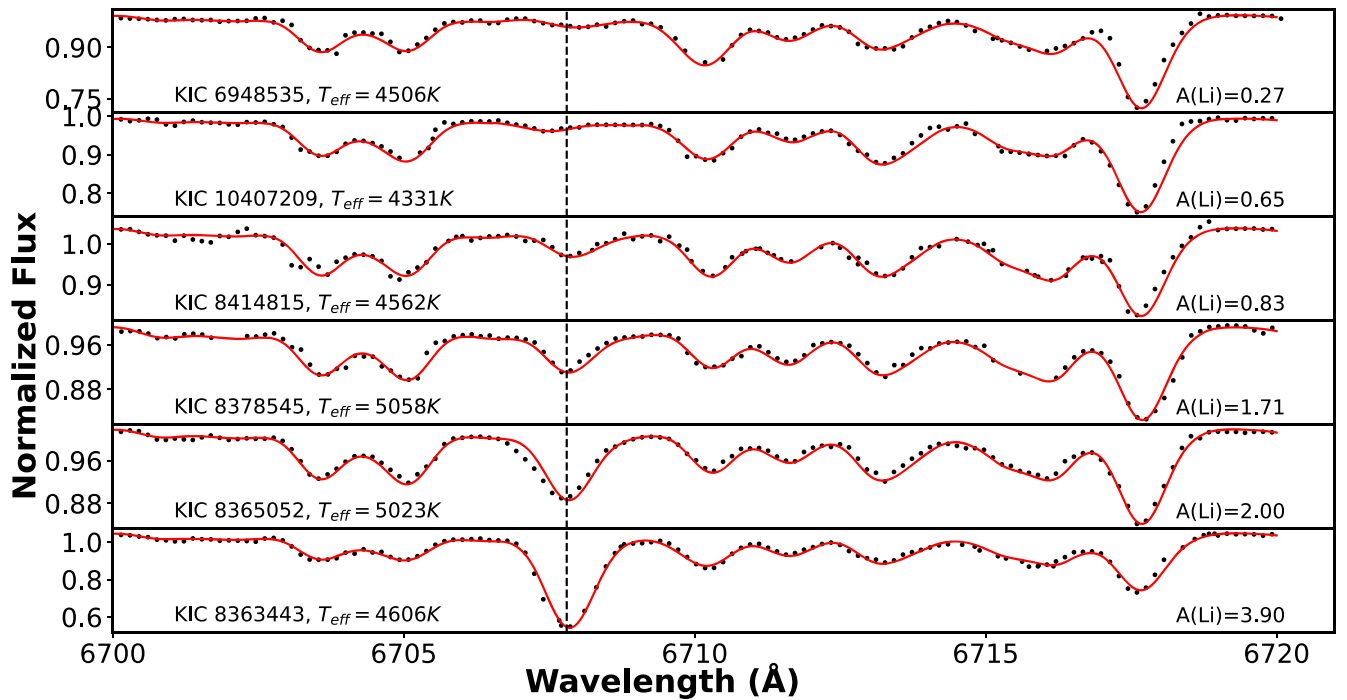
Figure 2. Determination of Li abundances for a few representative giants using spectrum synthesis around the Li 6707.8 Å resonance line.

The mean difference between ours and those in the literature is 0.35 dex with $\sigma = 0.02$. The evolutionary state of KIC 9907856, which we classified as a pRC from its period spacing, was undetermined by Yan et al. (2021). KIC 9596106, which was classified as an RGB, is also established to be a pRC star. The remaining 16 stars have the same evolutionary states as determined by Yan et al. (2021).

4. Discussion

The abundances of Li as a function of stellar mass for the entire sample are shown in Figure 3. The transition mass $M_{HeF} = 2\,M_\odot$ divides the giants into two groups: (a) pRCs ($\leqslant 2\,M_\odot$), which develop degeneracy at the core while evolving on RGB, and (b) sRCs ($> 2\,M_\odot$), which develop sufficient core temperatures to burn He at the core in convective conditions while evolving on the RGB, meaning no He flash in high-mass giants. In the case of low-mass giants, at the RGB tip, ignition of He near the central core results in a thermal runaway with He flashes, generating massive energy. Note that the adopted $2\,M_\odot$ demarcation is an approximate average value predicted by various studies with a range of 1.8–2.2 $M_\odot$ (Chiosi et al. 1992; Girardi 1999). The vertical region in Figure 3 indicates a possible range of masses that could separate pRC and sRC stars. (See Appendix B.) Though predictions suggest He flash generates a huge amount of energy, only a part of it goes into lifting the H-burning shell upwards and hence causes a sudden drop in luminosity. The bulk of the energy goes into removing the central degeneracy. Post He flash, stars settle at the RC with He burning at the core in convective conditions.

The key result from Figure 3 is that none of the sRC giants ($> 2\,M_\odot$) shows $A(Li)$ values more than that expected from the first dredge-up. The mean errors in $A(Li) = 0.19$ dex and mass $= 0.14\,M_\odot$ are indicated by an error cross in Figure 3. We have drawn a horizontal line at $A(Li) = 1.8$ dex, the expected maximum first dredge-up value for a star of mass 1.5 $M_\odot$
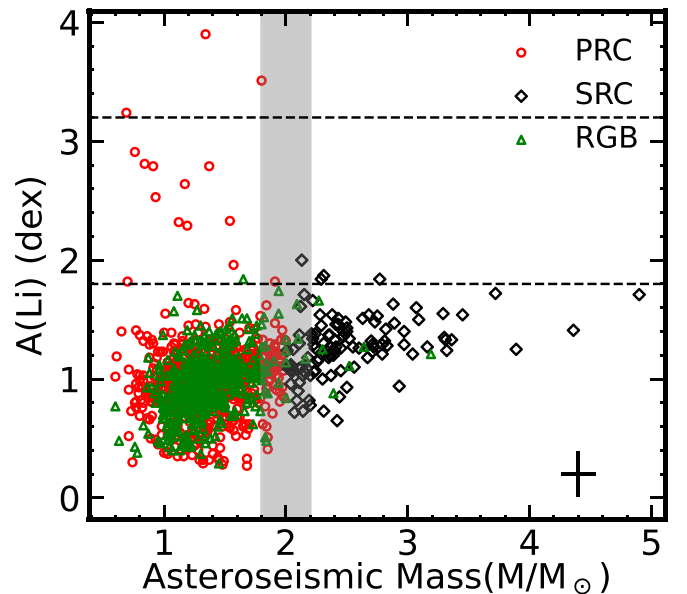

Figure 3. Li abundances of pRC, sRC, and RGB giants as a function of stellar mass. Horizontal lines mark the first dredge-up theoretical upper limit of A (Li) = 1.8 dex for a giant with $M = 1.5\,M_\odot$ and $A(Li) = 3.2$ dex for the super Li-rich giants. The error cross at the bottom right represents the mean errors in $A(Li)$ and mass.

(Iben 1967). We found similar maximum $A(Li)$ values for high-mass giants by computing models using Modules for Experiments in Stellar Astrophysics (MESA), an open-source 1D stellar evolution code (Paxton et al. 2011, 2019), based on the study by Schwab (2020a). Models are constructed for solar metallicity, as most of our giants are close to [Fe/H] = 0.0. Post first dredge-up, however, the models of high-mass giants show further depletion of Li as giants evolve to the sRC phase, though at a much slower rate than their low-mass pRC

Table 1
Derived and Adopted Parameters of Sample Giants

KIC	$T_{\rm eff}$ (K)	log g (dex)	[Fe/H] (dex)	ξ (km/s)	Mass ($M_\odot$)	A(Li)$_{\rm LTE}$ (dex)	$\Delta_{\rm NLTE}$ (dex)	$\Delta\nu$ (μHz)	ΔP ($\Delta\Pi_1$)[a] (s)	Evol.[b] Status
4136835	4909 ± 80	2.807 ± 0.008	−0.62 ± 0.15	1.4 ± 0.001	1.47 ± 0.08	0.99 ± 0.2	0.07	7.158 ± 0.011	73.67 ± 1.49(1)	0
4137210	4862 ± 80	2.978 ± 0.006	−0.35 ± 0.15	1.328 ± 0.001	1.35 ± 0.07	1.17 ± 0.2	0.15	9.841 ± 0.018	74.3 ± 0.65(2)	0
4243803	4646 ± 100	2.097 ± 0.033	0.05 ± 0.15	1.602 ± 0.002	2.39 ± 0.55	0.88 ± 0.17	0.32	1.882 ± 0.021	149.75 ± 5.17(1)	0
4345370	4872 ± 100	2.425 ± 0.007	−1.17 ± 0.15	1.69 ± 0.002	0.96 ± 0.05	1.12 ± 0.19	0.11	4.05 ± 0.012	76.08 ± 3.03(1)	0
4346319	4815 ± 100	2.578 ± 0.008	0.2 ± 0.15	1.483 ± 0.001	1.97 ± 0.14	1.41 ± 0.18	0.15	4.615 ± 0.045	315.1 ± 4.53(2)	1
4346893	4610 ± 100	2.419 ± 0.011	0.39 ± 0.15	1.53 ± 0.001	1.23 ± 0.11	1.02 ± 0.17	0.32	3.926 ± 0.032	289.4 ± 2.86(2)	1
4446405	4846 ± 100	2.688 ± 0.008	−0.13 ± 0.15	1.445 ± 0.001	1.58 ± 0.09	1.37 ± 0.19	0.15	5.75 ± 0.019	81.04 ± 6.15(1)	0
4633909	4753 ± 151	2.374 ± 0.012	−2.44 ± 0.3	1.706 ± 0.004	0.8 ± 0.09	0.69 ± 0.2	0.06	3.984 ± 0.062	315.1 ± 2.88(2)	1
4634108	4799 ± 100	2.642 ± 0.007	−0.03 ± 0.15	1.461 ± 0.001	1.27 ± 0.07	1.05 ± 0.21	0.15	5.618 ± 0.015	72.43 ± 37.85(1)	0
4634310	4748 ± 100	2.448 ± 0.013	0.22 ± 0.15	1.522 ± 0.001	1.37 ± 0.14	1.06 ± 0.2	0.32	4.027 ± 0.035	283.2 ± 2.76(2)	1

Notes.
[a] (1) ΔP (this work); (2) $\Delta\Pi_1$ (Vrard et al. 2016).
[b] 0—RGB, 1—pRC, 2 sRC.

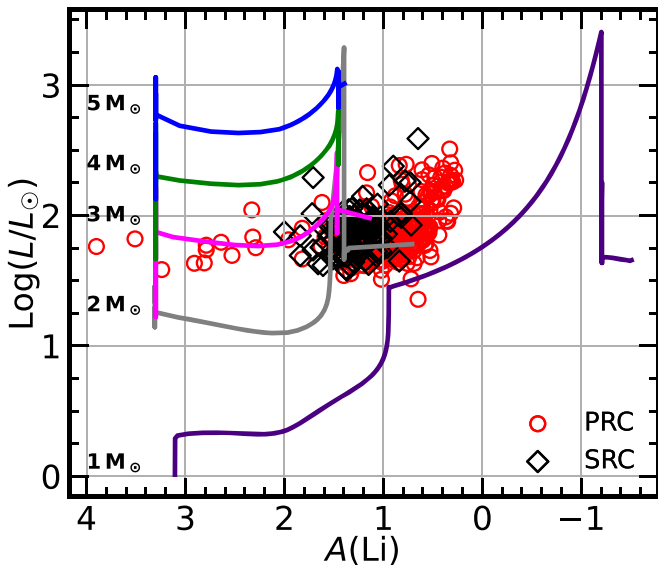(This table is available in its entirety in machine-readable form.)

Figure 4. The pRC and sRC giants in a luminosity and A(Li) plot superposed with MESA models of 1–5 $M_\odot$ giants. Note the many LRGs including SLRGs among pRCs and none among sRCs. Models show pRCs suffer severe depletion of Li during first dredge-up and also at the luminosity bump.

counterparts, which undergo extra mixing during the stars' luminosity bump evolution (Deepak & Lambert 2021).

The computed models for sRC giants yield A(Li) values between ≈ 0.7 and 1.6 dex, depending on mass (see Figure 4). The expected A(Li) values agree well with the observed values of sRC giants. However, three sRC giants show A(Li) values slightly higher, by ~ 0.1–0.3 dex, than the maximum model predictions of A(Li) = 1.6 dex. Given the uncertainties in the observed values of about 0.2 dex, the slightly higher values of Li in these giants may not be attributed to fresh enhancement but to their evolution. Also, high-mass giants begin burning He at the center well before they settle into the RC phase, which means some of these giants still can have a slightly higher Li abundance than those settled at RC (see Figure 4).

Importantly, unlike pRCs, none of the 109 sRCs in our sample are super Li rich (A(Li) = 3.2 dex). Slightly higher A(Li) (after taking into account the estimated ≈ 0.2 dex measurement uncertainty) for a couple of sRC giants is most probably due to insufficient mixing rather than enhancement. The observed range of A(Li) values among sRC giants is probably due to varying levels of depletion and, of course, the initial values of Li with which stars might have evolved off the main sequence. Further, one could notice from the data in Figure 3 and the models in Figure 4 that the range of A(Li) among sRC giants is relatively smaller compared to pRC giants. It is known that low-mass giants undergo severe depletion of Li due to first dredge-up and extra mixing near the luminosity bump. The high-mass giants neither have sufficient time for Li depletion, as they evolve faster nor do they have extra mixing at the luminosity bump. As shown in Figure 4, the 1 $M_\odot$ model suffers significant Li depletion both during first dredge-up and luminosity bump evolution. The lack of LRGs among sRCs provides another clue that He flash is the key source of Li enrichment among pRCs.

Previous attempts by Deepak & Reddy (2019) and Deepak & Lambert (2021) to understand the Li distribution as a function of mass could not resolve the issue either due to small sample sizes or unreliable mass determinations using stellar

evolutionary tracks. Most mass tracks overlap in the RC region in HRD, making it challenging to derive masses solely based on evolutionary tracks. Our study overcame these shortcomings by assembling a large sample common among the Kepler and LAMOST catalogs. The studies by Martell et al. (2021) and Zhou et al. (2022), however, suggest LRGs are a diverse population found among sRCs, pRCs, and also among RGB giants. The main differences between theirs and our study are the primary sample source and the method used to classify giants as RCs and RGBs. Our sample is sourced from the Yu et al. (2018) catalog of Kepler giants with oscillations identified. All giants in our study have direct measurement of ν_{max}, a key asteroseismic parameter for evolutionary phase determination and also have ΔP values measured directly from asteroseismic data. On the other hand, the primary source of the sample for the Martell et al. (2021) study is GALAH, and hence most of their sample giants do not have asteroseismic data. They identified giants as RCs and RGBs using stellar parameters that are proven to be ineffective for obvious reasons as RC and upper RGB regions overlap in the HRD. The study by Zhou et al. (2022) also shows a few SLRs among sRCs. Their sample is primarily drawn from the LAMOST survey similar to ours, but the classification of RCs and RGBs is based on neural networks. Unfortunately, there are no common giants between Martell et al. (2021) and ours. Zhou et al. (2022) did not publish their sample set. The other difference between ours and Martell et al. (2021) is their lower-mass cutoff of 1.7 $M_\odot$. However, this does not make a difference in the results shown in Figure 3. Among the many LRGs, only two are close to the adopted $M_{HeF} = 2 M_\odot$, an upper limit for the He-flash phenomenon that is possibly due to the metallicity effect (see Appendix B). It may be possible that giants might have lost 0.2 $M_\odot$ to 0.3 $M_\odot$ as they evolved to the RC phase (see Chanamé et al. 2022). This suggests that stars with an initial mass of about $\leqslant 2.2 M_\odot$ undergo He flash, implying only RC giants with a current mass of about 2 $M_\odot$ or less show Li enrichment.

5. Conclusion

We have used a large sample of RGB and RC stars with evolutionary phases classified using the asteroseismic diagram of ΔP–$\Delta \nu$ based on direct measurements of Kepler light curves. For the entire sample of 1240 giants (777 RCs and 463 RGBs), we derived Li abundances using spectral synthesis. We found no evidence of Li enrichment among sRCs. The observations conform with the theoretical A(Li) predictions for sRC giants of $M > 2 M_\odot$. We found all pRC giants, including 3 SLRGs and 11 giants with A(Li) > 1.8 dex, whose A(Li) values are much higher than that expected from models and their counterparts on the upper RGB. Also, we found no giant on the RGB with a Li abundance more than the upper limit of A(Li) = 1.8 dex expected from models for low-mass giants within the uncertainties. The lack of Li-rich giants among sRC stars is another clue that the He flash, which only occurs in low-mass giants, is a potential site for Li enrichment among low-mass giants. This result further adds to the growing evidence that Li enrichment occurs during the He flash. However, the transport process and mixing mechanism are yet to be explored. It would be worthwhile to combine carbon isotopic ratios ($^{12}C/^{13}C$) with lithium studies to understand mixing mechanisms.

This work has used data from the Yu et al. (2018) catalog available at http://vizier.u-strasbg.fr/viz-bin/VizieR?-source=J/ApJS/236/42. All spectra were taken from LAMOST public data release 7, operated and managed by National Astronomical Observatories, Chinese Academy of Sciences. We are grateful to the team of Stellar Classification Program (SCP) for the Kepler Mission. We acknowledge the utilization of MESA models assembled by Josiah Schwab. Schwab's input and output files are publicly available on Zenodo via Schwab (2020b).

Software: ASFGRID (Sharma et al. 2016), IRAF (Tody 1993), MOOG (Sneden 1973), MESA (Paxton et al. 2011, 2019), MESASDK 20.3.1 (Townsend 2020), py_mesa_reader (Wolf & Schwab 2017).

Appendix A
Measurement of Mixed-mode Period Spacing

Although all of our stars have known evolutionary phases in Yu et al. (2018), we derived period spacing to precisely infer the evolutionary phase based on the location of a star in the asteroseismic plot of $\Delta P - \Delta \nu$ (Bedding et al. 2011). Evolved stars show a rich spectrum of oscillation modes in the power density spectra (PDS), which are the radial, dipole, and quadruple modes. Dipole modes of evolved stars have mixed natures, i.e., they arise from coupling between p-modes in the envelope and g-modes in the core. Consecutive radial modes are equally spaced in frequency, and mixed dipole modes are approximately equally spaced in period (Tassoul 1980). Spacing of the period between consecutive mixed dipole modes has been used to identify different evolutionary phases of stars (Bedding et al. 2011; Mosser et al. 2012; Stello et al. 2013). For the measurement of period spacing, we retrieved Kepler photometric data from the MAST archive[4] using Lightkurve code[5] and converted the lightcurve into frequency space following the Lomb–Scargle periodogram method. We did a visual inspection of PDS for the identification of oscillation modes. Stars shows radial modes ($l = 0$), dipole modes ($l = 1$), and quadruple modes ($l = 2$). In each star, we identified three to five groups of mixed modes (see the top panel of Figure 5) and derived period spacing from consecutive mixed dipole modes. The mean value of the period spacing is adopted as the period spacing of stars and the standard deviation as the error of period spacing (Bedding et al. 2011; Stello et al. 2013; Singh et al. 2019).

To check the accuracy of our method, we compared ΔP values of six giants (2 each from the RGB, pRC, and sRC phases) measured by us with those from the Vrard et al. (2016) sample. As illustrated in Figure 6, our values are in good agreement as indicated by linear regression coefficients.
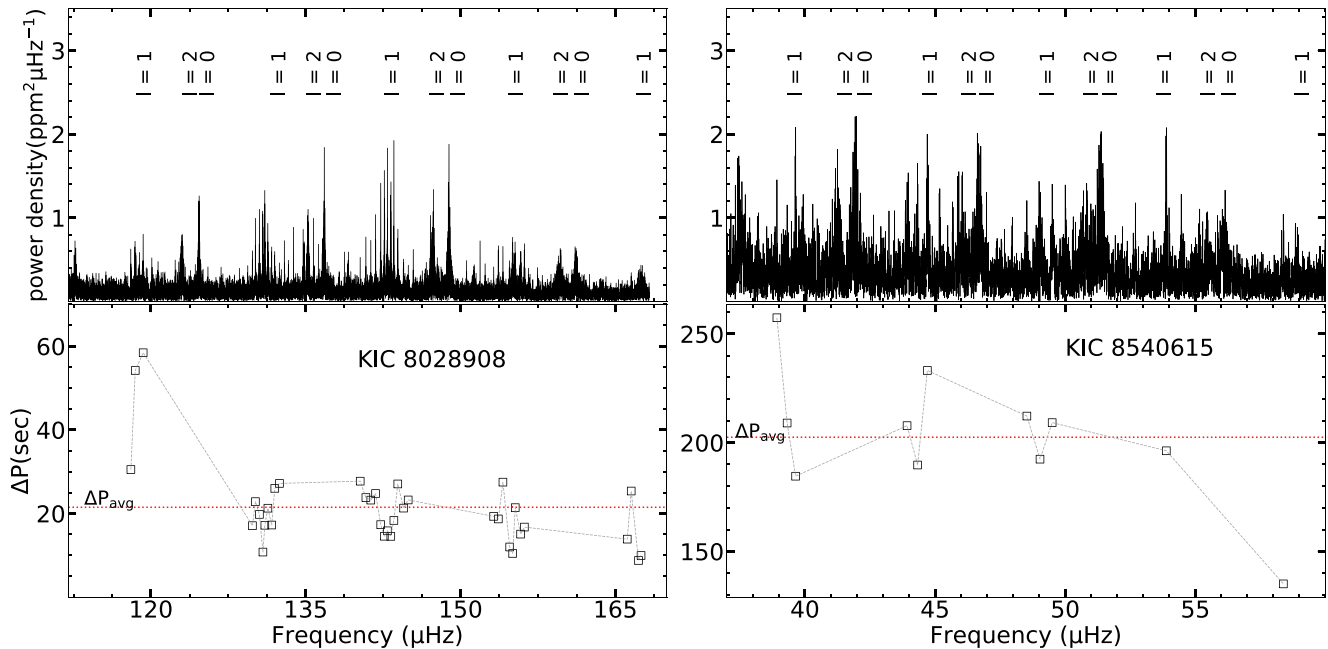

Figure 5. Measurement of period spacing. The top-left panel is the PDS of RGB star KIC 8028908, and the right panel is the PDS of the RC star KIC 8540615. Oscillation modes of $l = 0, 1, 2$ are identified and marked in the figure. The bottom panel is a demonstration of the measurement of mixed-mode ($l = 1$) period spacing (ΔP). The red dotted horizontal line is the average value of the period spacing in each bottom panel.
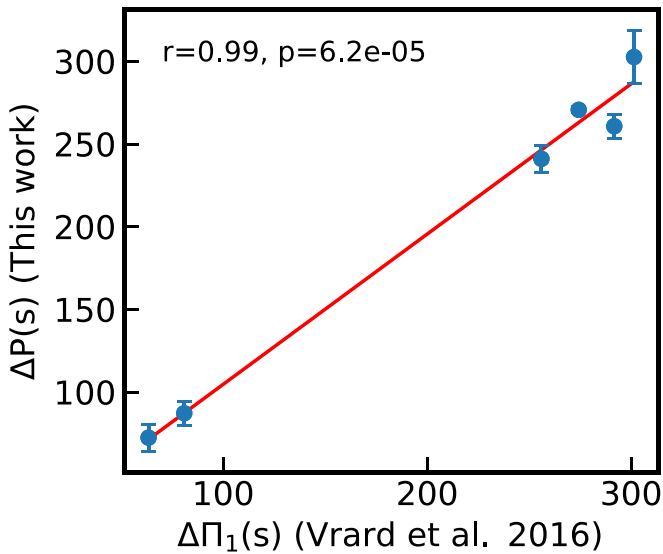
Figure 6. Average period spacing derived by us compared to values obtained by Vrard et al. (2016).

Appendix B
Variation of the Transition Mass in Flashing Stars

The range of masses for helium flash to occur in a star varies slightly with its composition. Masses range from 1.8 to $2.2\,M_\odot$ (Chiosi et al. 1992) or $2\text{–}2.5\,M_\odot$ (Girardi 1999). We used a median value of $2\,M_\odot$ to differentiate pRC and sRC stars. In Figure 3, there is one SLR star close to $M_{\mathrm{HeF}} = 2\,M_\odot$. To confirm its evolutionary status, we have plotted the helium core mass (M_c) and luminosity L from the main sequence to the end of the core helium-burning phase using a MESA stellar model of [Fe/H] = 0.14. The minimum is used to constrain the M_{HeF} value. From Figure 7,

1. KIC 8879518—$M_{\mathrm{Cl}} = 1.80\,M_\odot$, [Fe/H] = 0.14, $M_{\mathrm{HeF}} = 2.1\,M_\odot$

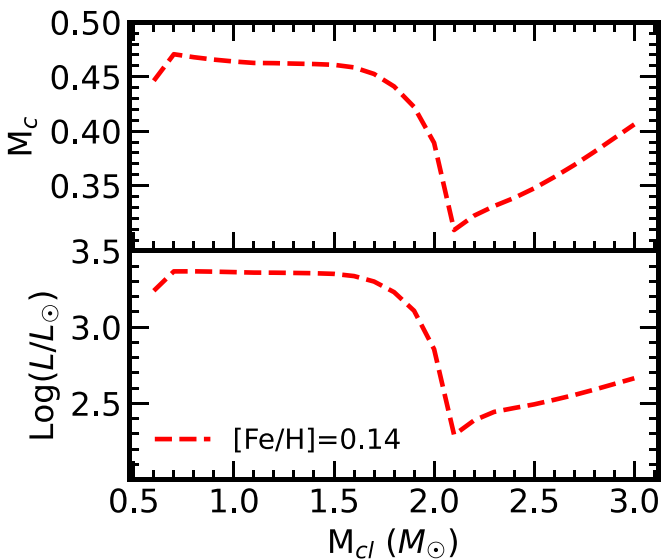Its $M_{\mathrm{Cl}} < M_{\mathrm{HeF}}$ and is confirmed to be an SLR pRC star.

Figure 7. He-core mass and luminosity as a function of stellar mass for two metallicities for stars evolving from the main sequence to core helium burning (CHeB) phases.

ORCID iDs

Anohita Mallick ⓘ https://orcid.org/0000-0002-4282-605X
Raghubar Singh ⓘ https://orcid.org/0000-0001-8360-9281
Bacham E. Reddy ⓘ https://orcid.org/0000-0001-9246-9743

References

Bedding, T. R., Mosser, B., Huber, D., et al. 2011, Natur, 471, 608
Boothroyd, A. I., & Juliana Sackmann, I. 1999, ApJ, 510, 232
Brown, J. A., Sneden, C., Lambert, D. L., & Dutchover, E., Jr. 1989, ApJS, 71, 293
Cameron, A. G. W., & Fowler, W. A. 1971, ApJ, 164, 111
Carlberg, J. K., Cunha, K., Smith, V. V., & Majewski, S. R. 2012, ApJ, 757, 109
Casey, A. R., Ho, A. Y. Q., Ness, M., et al. 2019, ApJ, 880, 125
Castelli, F., & Kurucz, R. L. 2003, in IAU Symp. 2010, Modelling of Stellar Atmospheres, ed. N. Piskunov, W. W. Weiss, & D. F. Gray (San Francisco, CA: ASP), A20
Cayrel, R. 1988, in IAU Symp. 132, The Impact of Very High S/N Spectroscopy on Stellar Physics, ed. G. Cayrel de Strobel & M. Spite (Dordrecht: Kluwer Academic), 345
Chanamé, J., Pinsonneault, M. H., Aguilera-Gómez, C., & Zinn, J. C. 2022, ApJ, 933, 58
Charbonnel, C., & Balachandran, S. C. 2000, A&A, 359, 563
Charbonnel, C., & Zahn, J.-P. 2007, A&A, 467, L15
Chiosi, C., Bertelli, G., & Bressan, A. 1992, ARA&A, 30, 235
Deepak, & Lambert, D. L. 2021, MNRAS, 507, 205
Deepak, & Reddy, B. E. 2019, MNRAS, 484, 2000
Denissenkov, P. A., Pinsonneault, M., & MacGregor, K. B. 2009, ApJ, 696, 1823
Gao, Q., Shi, J.-R., Yan, H.-L., et al. 2021, ApJ, 914, 116
García Pérez, A. E., Prieto, C. A., Holtzman, J. A., et al. 2016, AJ, 151, 144
Girardi, L. 1999, MNRAS, 308, 818
Holtzman, J. A., Hasselquist, S., Shetrone, M., et al. 2018, AJ, 156, 125
Iben, I., Jr. 1967, ApJ, 147, 624
Kumar, Y. B., Reddy, B. E., Campbell, S. W., et al. 2020, NatAs, 4, 1059
Kumar, Y. B., Reddy, B. E., & Lambert, D. L. 2011, ApJL, 730, L12
Lind, K., Asplund, M., & Barklem, P. S. 2009, A&A, 503, 541
Luo, A. L., Zhao, Y. H., Zhao, G., et al. 2022, yCat, 5156, 0
Martell, S. L., & Shetrone, M. D. 2013, MNRAS, 430, 611
Martell, S. L., Simpson, J. D., Balasubramaniam, A. G., et al. 2021, MNRAS, 505, 5340
Mosser, B., Goupil, M. J., Belkacem, K., et al. 2012, A&A, 540, A143
Paxton, B., Bildsten, L., Dotter, A., et al. 2011, ApJS, 192, 3
Paxton, B., Smolec, R., Schwab, J., et al. 2019, ApJS, 243, 10
Placco, V. M., Sneden, C., Roederer, I. U., et al. 2021, RNAAS, 5, 92
Schwab, J. 2020a, ApJL, 901, L18
Schwab, J. 2020b, A Helium-flash-induced Mixing Event Can Explain the Lithium Abundances of Red Clump Stars, Zenodo, doi:10.5281/zenodo.3960434
Sharma, S., Stello, D., Bland-Hawthorn, J., Huber, D., & Bedding, T. R. 2016, ApJ, 822, 15
Singh, R., Reddy, B. E., Bharat Kumar, Y., & Antia, H. M. 2019, ApJL, 878, L21
Singh, R., Reddy, B. E., Campbell, S. W., Kumar, Y. B., & Vrard, M. 2021, ApJL, 913, L4
Sneden, C., Afşar, M., Bozkurt, Z., et al. 2022, ApJ, 940, 12
Sneden, C. A. 1973, PhD thesis, Univ. of Texas, Austin
Stello, D., Huber, D., Bedding, T. R., et al. 2013, ApJL, 765, L41
Tassoul, M. 1980, ApJS, 43, 469
Tody, D. 1993, in ASP Conf. Ser. 52, Astronomical Data Analysis Software and Systems II, ed. R. J. Hanisch, R. J. V. Brissenden, & J. Barnes (San Francisco, CA: ASP), 173
Townsend, R. 2020, MESA SDK for Linux, v20.3.1, Zenodo, doi:10.5281/zenodo.3706650
Vrard, M., Mosser, B., & Samadi, R. 2016, A&A, 588, A87
Wallerstein, G., & Sneden, C. 1982, ApJ, 255, 577
Wolf, B., & Schwab, J. 2017, wmwolf/py_mesa_reader: Interact with MESA Output, v0.3.0, Zenodo, doi:10.5281/zenodo.826958
Xiang, M. S., Liu, X. W., Yuan, H. B., et al. 2015, MNRAS, 448, 822
Yan, H.-L., Zhou, Y.-T., Zhang, X., et al. 2021, NatAs, 5, 86
Yu, J., Huber, D., Bedding, T. R., et al. 2018, ApJS, 236, 42
Zhou, Y., Wang, C., Yan, H., et al. 2022, ApJ, 931, 136